Compressed higher-order structures facilitate human knowledge network learning

Xiangjuan Ren[1,2,6,7,8,], Muzhi Wang[1,2,3,8], Tingting Qin[4,8], Fang Fang[1,2,3], Aming Li[4,5,*], Huan Luo[1,2,3,*]

1. School of Psychological and Cognitive Sciences, Peking University, Beijing, China
2. PKU-IDG/McGovern Institute for Brain Research, Peking University, Beijing, China
3. Beijing Key Laboratory of Behavior and Mental Health, Peking University, Beijing, China
4. Center for Systems and Control, College of Engineering, Peking University, Beijing, China
5. Center for Multi-Agent Research, Institute for Artificial Intelligence, Peking University, Beijing, China
6. Max Planck Research Group NeuroCode, Max Planck Institute for Human Development, Berlin, Germany
7. Institute of Psychology, Universität Hamburg, Hamburg, Germany
8. Co-first author

*Corresponding authors:
Aming Li (A.L.)
amingli@pku.edu.cn
Huan Luo (H.L.)
huan.luo@pku.edu.cn

Abstract

Knowledge seeking is innate to human nature, yet integrating vast and fragmented information into a unified network is a daunting challenge, especially in the information explosion era. Graph theory describes knowledge as a network characterising relationships (edges) between isolated data (nodes). Accordingly, knowledge learning could be abstracted as network navigation through random walks, where local connections are gradually learned and integrated to form the global picture. To facilitate network learning, we develop a novel "compressive learning" approach that decomposes network structures into substructures based on higher-order inhomogeneity properties and designs pre-learning paths highlighting key substructures. Large-scale behavioural experiments and magnetoencephalography (MEG) recordings demonstrate its effectiveness and better network formation in human brains. Hypergraph-based computational models reveal that the pre-learning path helps establish the core network skeleton to efficiently accommodate late inputs. Overall, higher-order network structures are crucial to network learning and can be utilised to better "connect the dots".

Keywords: compressive learning; knowledge network; higher-order structure; hypergraph; dorsal ACC; graph learning; scale-free network; pre-learning path; inhomogeneity

Introduction

Humans are born to acquire knowledge. However, we often get lost in big data and miss forests, especially in the current information explosion era[1,2]. Individuals face significant challenges in constructing an integrated knowledge framework from enormous data far beyond their processing capacity[3,4]. Understanding the cognitive and computational mechanisms of knowledge acquisition and developing efficient learning approaches are vital to human societies[5–12].

Knowledge learning can be abstracted as navigation within a network, where fragmented data and their connections are represented by network nodes and edges linking nodes, respectively[13–15]. Accordingly, knowledge acquisition, in essence, is about extracting the network structure underlying a succession of fragmented inputs, *i.e.*, connecting the dots. Typical network learning relies on sequences generated from a random-walk path[16–18], whereby humans gradually learn the transitional relationship between consecutive items along the continuous path to infer the underlying whole network structure. Meanwhile, this learning procedure involves purely bottom-up, blind sampling of information, which is inefficient and time-consuming.

Recent interdisciplinary perspectives combining psychology, neuroscience, network science, and graph theory provide a valuable window to this challenge, suggesting that higher-order network structures, such as modular and inhomogeneity properties, help humans build more accurate mental representations of knowledge networks[15,19–22]. Moreover, these higher-order structures are also prevalent in real-world intelligent natural and engineering systems, including language[23,24], social networks[25], and the Internet[26], further implicating their roles in efficient information storage and transmission, a view also supported by theoretical analysis[27–29]. Therefore, higher-order network structures might be leveraged to promote network learning beyond the traditional random-walk path.

Here we draw on these findings and postulate two hypotheses. First, abstract network structures are compressible, like data such as images, audio, video, etc., and networks with higher-order properties would be more compact and thus more efficient to learn. Second and most crucially, given the compressibility of networks, we propose a “compressive learning” approach to facilitate network learning, a term borrowed from well-known "compressive sensing" in the signal processing field[30]. We hypothesise that a pre-learning shortcut path schematising higher-order network structures would set up a core skeleton to efficiently house later fragmented inputs. This “compressive learning” – brief training on shortcut paths – would be more effective than traditional random-walk paths.

We focused on inhomogeneity, a well-known but less studied higher-order network structure, to examine the hypotheses[31–35]. We conducted two large-scale behavioural experiments ($N > 400$) and confirmed the role of higher-order properties and the effectiveness of "compressive learning" in network learning. Magnetoencephalography (MEG) recordings demonstrate that the compressive pre-learning path promotes subsequent formation of network structures in human brains. Finally, we developed a mathematical model based on hypergraph theory to illustrate the underlying computational mechanisms, revealing that compressive learning helps establish the core network skeleton to efficiently accommodate late inputs.

Results

Behavioural paradigm for knowledge network learning

The behavioural task was adapted from previous network learning paradigms[36]. A series of 16-node, undirected and unweighted networks was created in which the 1-step transition probabilities between individual nodes are pre-determined accordingly (Figure 1a). 16 black-and-white images were randomly assigned to the 16 nodes of the network (Figure 1a, left), constituting the to-be-learned artificial knowledge network. Next, image sequences were generated based on a random walk path within the network (Figure 1b, right). Subjects performed continuous prediction through trial-and-error without being told about the actual underlying network. On each trial, subjects were presented with a Cue image and predicted its succeeding image from the Target-Distractor image pair (Figure 1b, left), and the Target image on the current trial would automatically become the Cue image in the next trial (Figure 1b, middle). We monitored subjects' mouse trajectories during decision-making and performed a trial-wise binary classification analysis to quantify network learning performance (Figures 1c and S3). Specifically, the mouse cursor would be closer to the target than to the distractor if subjects had learnt the transitional relations. Moreover, we employed a "hint system" and a "coin system" to motivate learning (see details in Methods and Figure S2).

Higher-order structure impacts knowledge network learning

Experiment 1 ($N = 160$) examined the impacts of higher-order network structures (*i.e.*, inhomogeneity) on human network learning. To this end, we created four types of 16-node networks (Figure 1a): Lattice (pink), Random (green), Small-world (blue), Scale-free (orange). They are matched in the number of nodes (16), edges (32), and the average number of connections (average node degree, 4), but have diverse inhomogeneity properties, *i.e.*, the distribution of node degree (Figures 1a and S1). The Lattice network has the lowest inhomogeneity since every node has four connections. Random and Small-world networks are more inhomogeneous with approximate normal node-degree distribution. The Scale-free network exhibits the highest inhomogeneity, *i.e.*, the power-law node degree distribution (a few nodes with a large number of connections). The same 16 images were embedded into the four networks and shuffled across subjects to avoid image confounding. Theoretical analyses show that scale-free networks are more compressible than other networks (see Figures S13 a-b), thus suggesting their superior learnability.

A total of 160 subjects participated in Experiment 1 and were randomly assigned

to four groups (40 subjects each). Each group learned one of the four networks based on image sequences generated by random-walk paths within the corresponding network (Figure 1a-b). Every subject completed 1,000 trials divided into 5 blocks. A trial-wise binary classification analysis of mouse trajectories was performed to evaluate the four groups' learning performance (Figure 1c). As shown in Figure 1d-e, all groups exhibited above-chance prediction before hints, *i.e.*, moving the mouse toward the target rather than the distractor. Interestingly, the Scale-free group showed the highest prediction performance (Figures 1e, S4-6), supporting our first conjecture that knowledge networks with higher-order structure, *i.e.*, inhomogeneity, have better learnability. A generalised linear mixed effects model (GLMM1), by controlling recency, node-degree and other confounders, further supports the superiority of the Scale-free network (ANOVA from GLMM1 with likelihood ratio tests, main effect of network and trial numbers: $\chi^2(3) = 143.92$, $p < 0.001$, $\chi^2(1) = 26.71$, $p < 0.001$, interaction effect between network and trial numbers: $\chi^2(3) = 4.45$, $p = 0.216$; post-hoc comparisons with Bonferroni correction from GLMM1, Scale-free vs. Lattice: $z = 10.63$, $p < 0.001$; Scale-free vs. Random: $z = 9.81$, $p < 0.001$; Scale-free vs. Small-world: $z = 8.68$, $p < 0.001$; see the full statistical reports in the Supplememtary Information). Overall, network structure indeed impacts human network learning, and networks with higher-order inhomogeneity properties (*i.e.*, scale-free networks) are more compact and easier to learn.

"Compressive learning": priming higher-order structure facilitates network learning

Experiment 2 (N = 240) examined the "compressive learning" idea proposing that briefly priming the higher-order structure would facilitate subsequent learning. We focused on the Scale-free network as it is endowed with higher-order inhomogeneity structure that could be leveraged to develop pre-learning paths.

Notably, all nodes in a scale-free network could be sorted by their node-degree in ascending order, referred to as leaf nodes (small circle) and hub nodes (large circle) (Figure 2a, left). Typical random-walk paths, as in Experiment 1, visit all nodes in a probabilistic manner. To emphasise the inhomogeneity of network structure during pre-learning, we re-organised the 200-length image sequence generated from random-walk path (RandomWalk) according to each image's node-degree in descending or ascending order, yielding two new pre-learning paths: HubToLeaf and LeafToHub (Figure 2a-b). Therefore, the three pre-learning paths (RandomWalk, HubToLeaf, LeafToHub) contain the same images with the same frequencies but in different orders. Specifically, the HubToLeaf group learned relationships between hubs and their neighbours first,

then secondary hubs and their neighbours, and finally leaf nodes. In contrast, the LeafToHub group learned in reverse order, starting with relationships between leaf nodes and their neighbours, and last learning hub nodes and their links. In other words, the HubToLeaf and LeafToHub paths break the original probabilistic continuity of the RandomWalk path, highlighting the inhomogeneity structure of the to-be-learned knowledge network to different extents. In light of Hub's pivotal role in inhomogeneity and the primacy effect during learning, we hypothesise that the HubToLeaf pre-learning path would assist in building the core scaffold of the network structure to facilitate subsequent learning, compared to RandomWalk and LeafToHub paths.

A total of 240 new subjects participated in Experiment 2 and were randomly assigned to three groups (80 subjects each; 2 were removed from the RandomWalk group). Each group was exposed to image sequences generated by one of the three pre-learning paths – RandomWalk, HubToLeaf, LeafToHub (200 trials; Learning I), followed by identical RandomWalk image sequences (800 trials; Learning II) (Figure 2a, right). Notably, only Learning II performance was compared between groups to examine the pre-learning paths' impacts. The same trial-wise classification analysis of mouse trajectories as Experiment 1 was performed to evaluate learning performance, and all groups exhibited above-chance prediction before hints (Figure 2c). The 800 trials of Learning II were divided into 8 bins (100 trials each) to access the learning course. While all three groups showed similar performance at the beginning, HubToLeaf gradually outperformed the other two and maintained its lead thereafter (Figure 2d; see the statistical reports from GLMM2.1 in the Supplementary Information). The overall performance averaged across all trials in Learning II followed the similar pattern, further confirming the superiority of the HubToLeaf group (Figure 2e; ANOVA from GLMM2.2 with likelihood ratio tests, main effect of group and trial numbers: $\chi^2(2) = 124.68$, $p<0.001$, $\chi^2(1) = 22.71$, $p < 0.001$, interaction effect between group and trial numbers: $\chi^2(2) = 9.35$, $p = 0.009$; post-hoc comparisons with Bonferroni correction from GLMM2.2, HubToLeaf vs. RandomWalk: $z = 10.72$, $p < 0.001$; HubToLeaf vs. LeafToHub: $z = 8.03$, $p < 0.001$; RandomWalk vs. LeafToHub: $z = -2.77$, $p = 0.017$). An in-laboratory experiment replicated the results (See Figure S7). Taken together, the results support the "compressive learning", *i.e.*, pre-learning paths that prime the higher-order inhomogeneity structure (HubToLeaf path) facilitates subsequent network learning.

Dorsal ACC tracks network structure formation facilitated by "compressive learning"

After confirming the effectiveness of "compressive learning", we examined the underlying neural mechanism using MEG recordings. A total of 40 new subjects were recruited and assigned randomly to the HubToLeaf (purple) or LeafToHub (green) groups (20 subjects each), using the same paradigm as Experiment 2 with minor modifications due to MEG limitations (Figure 3a and Figure S2b). The two groups learned HubToLeaf or LeafToHub image sequences during Learning I, followed by identical RandomWalk image sequences (600 trials) during Learning II. Importantly, only neural activities during Learning II were analysed and compared between the groups.

To examine neural representations of network structure during Learning II, we performed representational similarity analyses (RSA) on individuals' neural responses after cue images (Figure 3b). Specifically, the multivariate neural dissimilarities between cue-elicited neural responses (neural RDM; Figure 3b) are hypothesised to reflect the transitional distance between (cue) nodes within the learned network (model RDM; Figure 3c). At each time and for each subject, the neural RDM was regressed by the model RDM, yielding the time-resolved representational strength course of the network structure. Notably, due to shuffled combinations of images and nodes across subjects, any differences observed here cannot be explained by cue images. As shown in Figure 3d, after the onset of the cue image, both groups exhibited neural correlates of network structure (black line). Meanwhile and most importantly, during the subsequent blank interval before target and distractor images (Figure S2b), the HubToLeaf group demonstrated stronger network representations than the LeafToHub group (LMM1 with cluster-based permutation test, right-sided, p=0.042), consistent with behavioural findings. Further control analyses within this time-of-interest (~1.2 s after cue onset; orange shaded area) confirmed that the HubToLeaf group established better neural representations of network structure than the LeafToHub group. First, the HubToLeaf group showed superior neural representation than the LeafToHub group for both Hub-related and Leaf-related substructures (Figure 3h; LMM1, right-sided, hub-related, $\beta = 0.012$, $t(44.48) = 2.12$, $p = 0.040$; leaf-related, $\beta = 0.007$, $t(43.85) = 2.25$, $p = 0.029$). This suggests that the better neural representation of network structure in the HubToLeaf group does not just arise from the Hub-related substructure but applies to the whole network. Second, multidimension scaling (MDS) analysis of neural RDMs revealed clear hierarchical organisation of nodes (Figure 3f) that resembles the ground-truth network structure (Figure 3e) for the HubToLeaf group, but not for the LeafToHub group (Figure 3g, see Figure S9 for distance analyses). Notably, to limit movements

during MEG recordings, subjects were instructed to press buttons instead of continuously moving the mouse as in Experiment 2. As a consequence, the less sensitive button response did not show difference between the two groups behaviourally (Figure S8; ANOVA from GLMM2.2 with likelihood ratio tests, main effect of group and trial numbers: $\chi^2(2)$ =0.02, p = 0.884, $\chi^2(1)$ =22.92, p = 0.001, interaction effect between group and trial numbers: $\chi^2(2) = 1.72$, p = 0.190).

Finally, we projected sensor-level data within the time-of-interest window (Figure 3d) into source space and performed the same RSA analysis to locate brain regions that differentiate the two groups in network learning (Figure 3i). The dorsal anterior cingulate cortex (ACC) showed significant differences in neural representation of network structure between groups (Figure 3j; LMM1, *FDR* correction for whole-brain searchlight, peak p = 0.004, MNI X=0, Y=-5, Z=45; see Figure S12 for ROI-based RSA of the hippocampus). This was not accompanied by differences in activity strengths (Figure S11). Moreover, the early network representation shared by both HubToLeaf and LeafToHub groups after the cue image involves brain regions including bilateral medial frontal cortex and right postcentral cortex (Figure S10, Table S1). Overall, dorsal ACC tracks how pre-learning paths influence network structure formation in human brains.

Hypergraph-based theoretical model explains "compressive learning"

Finally, we developed theoretical models based on graph theory to illustrate the computational mechanisms of compressive network learning. Specifically, images and their 1-step transitional relationship in the network could be characterised by an adjacency matrix $\mathbf{A}$, which encodes the to-be-learned network structure.

We first modelled the impacts of higher-order structure on network learning (Experiment 1), where four groups were presented with image sequence generated from random-walk path within different types of networks. When making choices between target and distractor images in the prediction task, they would recall previously encountered image sequences, potentially inducing biases or errors (Figure 4a). The relational bias between the current image and previously encountered images could be captured by the Boltzmann distribution ($P(\Delta n) \propto e^{-\beta \Delta n}$), where Δn is their in-between distance in the sequence (*i.e.*, between cue image i and images j, k) and β indicates the learning efficiency[37]. In the asymptotic analysis, the subjects' learned relational network ($\widehat{\mathbf{A}}$) is the theoretical estimation of the true network ($\mathbf{A}$) by combining all possible random walks of various lengths, namely, $\widehat{\mathbf{A}} = \sum_{\Delta n=0}^{\infty} P(\Delta n)\mathbf{\Pi}\mathbf{T}^{\Delta n+1}$, where $\mathbf{T}$ is the true transition probability matrix of the underlying network and $\mathbf{\Pi}$ captures the probability of images appearing in the sequence (see Methods). To optimise parameter

estimation, we fitted the overall learning efficiencies (β) using participants' final choices across all trials in Experiment 1 (maximum likelihood estimation). Thus, we could use the estimated β to predict the time course of the learning performance (divided into 5 bins) for each of the four groups, which showed a high consistency between data and model predictions (Figure 4b). Next, we examined the generic influence of inhomogeneity on network learning through simulation. To this end, we generated 5,000 synthetic networks for each network (lattice, random, small-world and scale-free networks), and calculated the resulting Kullback-Leibler (KL) divergence between the true network ($\mathbf{A}$) and the learned network ($\widehat{\mathbf{A}}$) with different β. Notably, a lower KL divergence denotes higher similarities between $\mathbf{A}$ and $\widehat{\mathbf{A}}$, and thus a better learning performance. As shown in Figure 4c, the scale-free networks exhibited the persistently best learning performance regardless of β, supporting the influence of higher-order network structure on learnability.

We next modelled the compressive learning process and explored the impacts of pre-learning paths on subsequent network learning (Experiment 2). As described earlier, Experiment 2 comprises two stages: Learning I (200 trials, pre-learning path) and Learning II (800 trials, random-walk path). With regards to Learning I, we leveraged the concept of the hypergraph with hyperedges (E_i) composed of node i and a set of nodes connected to it (Figure 4d), and constructed the frequency-modified adjacency matrix ($\mathbf{A}_{\mathrm{h}}$) of the hypergraph. Figure 4e illustrates the hypergraph-based network learning via different pre-learning paths. For the to-be-learned Scale-free network ($\mathbf{A}$), the two pre-learning paths gradually form hyperedges in reverse order, from Hub-related to Leaf-related hyperedges and vice versa for the HubToLeaf and LeafToHub groups, respectively. The network structure ($\widehat{\mathbf{A}}_{\mathrm{h}}$) shaped in the HubToLeaf group exhibits higher similarity to the true network ($\mathbf{A}$) than that in the LeafToHub group during pre-learning exposures. This signifies the former path's beneficial role in conveying essential network structure.

Learning II was characterised using the same model as Experiment 1 given the random-walk path. Learning I and Learning II models were then combined by weighted average as the overall network learning performance:

$$\mathbf{C} = \alpha^p \widehat{\mathbf{A}}_{\mathrm{h}} + (1 - \alpha^p)\widehat{\mathbf{A}},$$

where $\widehat{\mathbf{A}}_{\mathrm{h}}$ and $\widehat{\mathbf{A}}$ denote the learned network during Learning I and Learning II, respectively, and α^p denotes the weights. The weighted models showed good fitting performance for all three pre-learning path groups in Experiment 2 (Figure 4f). Based on this model, we next simulated the learning performance of HubToLeaf and LeafToHub groups with different learning efficiency parameters β_1 (Learning I) and β_2 (Learning II). As shown in Figure 4g, simulation results supported the general

superiority of HubToLeaf over LeafToHub group, *i.e.*, smaller KL divergence for the former group across a wide range of β_1 and β_2 combinations. Overall, hypergraph-based theoretical models suggest that HubToLeaf pre-learning forms the core hyperedges of the scale-free network by emphasising the higher-order inhomogeneity structure to facilitate subsequent network learning (see Figure S15).

Discussion

We live in an era of information explosion, where data is overwhelming, fragmented and unstructured, making humans' innate desire for knowledge challenging. Here we propose a "compressive learning" approach to condense the core schema of knowledge network structure into pre-learning paths. We confirm the approach in two large-scale behavioural experiments and demonstrate the underlying neurobiological and computational principles. Other fields such as education and machine learning may also benefit from our findings.

The core idea of "compressive learning" is to decompose abstract network structures into substructures of varying importance. This is motivated by "compressive sensing" whereby signals are reduced into a few dimensions to reconstruct the original signals [30,38]. Unlike previous studies that leverage the underlying structure to facilitate learning of successions of items, "compressive learning" directly decomposes the network structure into substructures based on higher-order properties (*i.e.*, inhomogeneity here). Specifically, hub nodes and their connections constitute substructures that carry more substantial information about the overall network structure, whereas leaf nodes and their links comprise less informative substructures. Therefore, given the primacy effect in learning and memory, early training of key substructures such as hub-related higher-order structures using HubToLeaf pre-learning path would optimise network learning. The computational mechanism is further illustrated by the hypergraph-based model where substructures are quantified as hyperedges. The “compressive learning” idea also echoes constructivism theory in education, that is, learners do not passively acquire knowledge but construct their understanding by integrating newly acquired information with their existing knowledge[12,39,40]. Here, the hub-to-leaf pre-learning path would help the early formation of key network structures, allowing new inputs to be better incorporated into existing knowledge framework.

We provide empirical evidence that higher-order network structure is crucial to network learning, *i.e.*, inhomogeneous networks are better learned, and earlier exposure to hub-related higher-order structure enhances both network learning performance and neural representation of network structure in human brains. Humans spontaneously track associations between consecutive items, known as statistical learning[41,42], and ideally, these local structures could merge into a comprehensive network[28,37]. However, such local-based learning is implausible since humans have limited cognitive and memory resources. Here, both experimental and theoretical studies suggest that higher-order network structures that represent global properties of nodes and edges contribute

significantly to human learning[15,36]. It is interesting to note that these higher-order properties are also prevalent in real-world networks[15,24,29,43,44], further implicating their importance in mediating efficient information storage.

Dorsal ACC tracks the formation of networks mediated by "compressive learning". Interestingly, the two pre-learning groups showed different neural correlates of network structure at a later time point, right before decision making and occurring at dorsal ACC. Many adaptive behaviours are mediated by ACC[45], such as hierarchical decision-making[46], foraging[47], meta-learning[48], exploration-exploitation balance[49], and learning rates encoding[50]. ACC also displays representation of task contexts[51] and future plans in structured environments[52]. Recent rat recordings revealed a long latency of the ACC's firing, suggesting that the ACC integrates error signals projected from the frontal cortex to contribute to higher-level decisions[53]. Our work is thus consistent with these findings and extends the ACC's role to learning complex network structures.

“Compressive learning” is distinct from current curriculum-learning, which is becoming increasingly popular in artificial agent training and refers to the process of learning from easy to hard (see ref. 54 for a review). In contrast, the HubToLeaf path is actually a hard-to-easy pre-training course, given large amounts of connections to hub nodes to learn at the beginning. Moreover, unlike previous models focusing on sequence statistical properties, we explicitly model higher-order network properties as hyperedges within the hypergraph framework. Future work could combine graph theory and classical learning algorithms to uncover complex network learning principles.

Data and code availability

All data and codes will be made publicly available upon acceptance of the paper.

Acknowledgments

This work was supported by the National Science and Technology Innovation STI2030-Major Project 2021ZD0204100 (2021ZD0204103 to H.L.), National Key Research and Development Program of China (2022YFA1008400 to A.L.), National Natural Science Foundation of China (31930052 to H.L., 62173004 to A.L.), SMP-IDATA Chenxing Youth Fund (to A.L.). We thank the Center for MRI Research at Peking University in Beijing, China, for assistance with data acquisition. We also thank Prof. Nai Ding and Prof. Jian Li for their comments on the manuscript and Dr. Haoyang Lu for statistical consulation.

Author contributions

X.R., A.L., and H.L. originally conceived the study. X.R. and M.W. performed the experiments. X.R., M.W., and T.Q. analysed the data. T.Q., A.L., and H.L. performed theoretical analyses. X.R., M.W., T.Q., F.F., A.L., and H.L. wrote the paper.

Declaration of interests

The authors declare no competing interests.

References

1. Goldie, J. G. S. Connectivism: A knowledge learning theory for the digital age? *Med. Teach.* **38**, 1064–1069 (2016).
2. Siemens, G. Connectivism: A Learning Theory for the Digital Age. *International Journal of Instructional Technology and Distance Learning* **2**, (2005).
3. Miller, E. K. & Buschman, T. J. Working Memory Capacity: Limits on the Bandwidth of Cognition. *Daedalus* **144**, 112–122 (2015).
4. Miller, G. A. The magical number seven, plus or minus two: Some limits on our capacity for processing information. *Psychol. Rev.* **63**, 81–97 (1956).
5. Bengio, Y., Louradour, J., Collobert, R. & Weston, J. Curriculum learning. in *Proceedings of the 26th Annual International Conference on Machine Learning* 41–48 (Association for Computing Machinery, New York, NY, USA, 2009). doi:10.1145/1553374.1553380.
6. Flesch, T., Balaguer, J., Dekker, R., Nili, H. & Summerfield, C. Comparing continual task learning in minds and machines. *Proc. Natl. Acad. Sci. U.S.A.* **115**, E10313–E10322 (2018).
7. Miller, A. M. P. *et al.* Emergence of a predictive model in the hippocampus. *Neuron* **111**, 1952-1965.e5 (2023).
8. Nelli, S., Braun, L., Dumbalska, T., Saxe, A. & Summerfield, C. Neural knowledge assembly in humans and neural networks. *Neuron* S0896627323001186 (2023) doi:10.1016/j.neuron.2023.02.014.
9. Tervo, D. G. R., Tenenbaum, J. B. & Gershman, S. J. Toward the neural implementation of structure learning. *Curr. Opin. Neurobiol.* **37**, 99–105 (2016).
10. Tse, D. *et al.* Schemas and Memory Consolidation. *Science* **316**, 76–82 (2007).
11. Zhou, D., Lydon-Staley, D. M., Zurn, P. & Bassett, D. S. The growth and form of knowledge networks by kinesthetic curiosity. *Curr. Opin. Behav. Sci.* **35**, 125–134 (2020).
12. Van Kesteren, M. T. R., Ruiter, D. J., Fernández, G. & Henson, R. N. How schema and novelty augment memory formation. *Trends Neurosci.* **35**, 211–219 (2012).
13. Mark, S., Moran, R., Parr, T., Kennerley, S. W. & Behrens, T. E. J. Transferring structural knowledge across cognitive maps in humans and models. *Nat. Commun.* **11**, 4783 (2020).
14. Tenenbaum, J. B., Kemp, C., Griffiths, T. L. & Goodman, N. D. How to Grow a Mind: Statistics, Structure, and Abstraction. *Science* **331**, 1279–1285 (2011).
15. Lynn, C. W. & Bassett, D. S. How humans learn and represent networks. *Proc. Natl. Acad. Sci. U.S.A.* **117**, 29407–29415 (2020).
16. Da Fontoura Costa, L. Learning about knowledge: A complex network approach. *Phys. Rev. E* **74**, 026103 (2006).
17. Garvert, M. M., Dolan, R. J. & Behrens, T. E. A map of abstract relational knowledge in the human hippocampal–entorhinal cortex. *eLife* **6**, e17086 (2017).
18. Schapiro, A. C., Rogers, T. T., Cordova, N. I., Turk-Browne, N. B. & Botvinick, M. M. Neural representations of events arise from temporal community structure. *Nat. Neurosci.* **16**, 486–492 (2013).
19. Battiston, F. *et al.* Networks beyond pairwise interactions: Structure and dynamics. *Phys. Rep.* **874**, 1–92 (2020).
20. Dehaene, S., Meyniel, F., Wacongne, C., Wang, L. & Pallier, C. The Neural Representation of Sequences: From Transition Probabilities to Algebraic Patterns and Linguistic Trees. *Neuron* **88**, 2–19 (2015).
21. Stachenfeld, K. L., Botvinick, M. M. & Gershman, S. J. The hippocampus as a predictive map. *Nat. Neurosci.* **20**, 1643–1653 (2017).
22. Wing, E. A., Burles, F., Ryan, J. D. & Gilboa, A. The structure of prior knowledge enhances memory in experts by reducing interference. *Proc. Natl. Acad. Sci. U.S.A.* **119**, e2204172119

(2022).
23. Borge-Holthoefer, J. & Arenas, A. Semantic Networks: Structure and Dynamics. *Entropy* **12**, 1264–1302 (2010).
24. Masucci, A. P., Kalampokis, A., Eguíluz, V. M. & Hernández-García, E. Wikipedia Information Flow Analysis Reveals the Scale-Free Architecture of the Semantic Space. *PLOS ONE* **6**, e17333 (2011).
25. Newman, M. *Networks: An Introduction*. (Oxford University Press, 2010). doi:10.1093/acprof:oso/9780199206650.001.0001.
26. Faloutsos, M., Faloutsos, P. & Faloutsos, C. On power-law relationships of the Internet topology. *SIGCOMM Comput. Commun. Rev.* **29**, 251–262 (1999).
27. Lynn, C. W. & Bassett, D. S. Quantifying the compressibility of complex networks. *Proc. Natl. Acad. Sci. U.S.A.* **118**, e2023473118 (2021).
28. Qian, W. *et al.* Optimizing the human learnability of abstract network representations. *Proc. Natl. Acad. Sci. U.S.A.* **119**, e2121338119 (2022).
29. Rosvall, M. & Bergstrom, C. T. Maps of random walks on complex networks reveal community structure. *Proc. Natl. Acad. Sci. U.S.A.* **105**, 1118–1123 (2008).
30. Donoho, D. L. Compressed sensing. *IEEE Trans. Inform. Theory* **52**, 1289–1306 (2006).
31. Kahn, A. E., Karuza, E. A., Vettel, J. M. & Bassett, D. S. Network constraints on learnability of probabilistic motor sequences. *Nat. Hum. Behav.* **2**, 936–947 (2018).
32. Benson, A. R., Gleich, D. F. & Leskovec, J. Higher-order organization of complex networks. *Science* **353**, 163-166 (2016).
33. Lambiotte, R., Rosvall, M. & Scholtes, I. From networks to optimal higher-order models of complex systems. *Nat. Phys.* **15**, 313-320 (2019).
34. Majhi, S., Perc, Matjaž. & Ghosh, D. Dynamics on higher-order networks: A review. *J. R. Soc. Interface* **19**, 20220043 (2022).
35. Battiston, F. *et al.* The physics of higher-order interactions in complex systems. *Nat. Phys.* **17**, 1093–1098 (2021).
36. Ren, X., Zhang, H. & Luo, H. Dynamic emergence of relational structure network in human brains. *Prog. Neurobiol.* **219**, 102373 (2022).
37. Lynn, C. W., Kahn, A. E., Nyema, N. & Bassett, D. S. Abstract representations of events arise from mental errors in learning and memory. *Nat. Commun.* **11**, 2313 (2020).
38. Baraniuk, R. G. Compressive Sensing. *IEEE Signal Processing Magazine* **24**, 118–121 (2007).
39. Derry, S. Cognitive schema theory in the constructivist debate. *Educ. Psychol.* **31**, 163–174 (1996).
40. Gilboa, A. & Marlatte, H. Neurobiology of Schemas and Schema-Mediated Memory. *Trends Cogn. Sci.* **21**, 618–631 (2017).
41. Saffran, J. R., Aslin, R. N. & Newport, E. L. Statistical Learning by 8-Month-Old Infants. *Science* **274**, 1926–1928 (1996).
42. Frost, R., Armstrong, B. C. & Christiansen, M. H. Statistical learning research: A critical review and possible new directions. *Psychol. Bull.* **145**, 1128–1153 (2019).
43. Lin, M. & Li, N. Scale-free network provides an optimal pattern for knowledge transfer. *Physica A* **389**, 473–480 (2010).
44. Lynn, C. W., Holmes, C. M. & Palmer, S. E. Emergent scale-free networks. Preprint at https://doi.org/10.48550/arXiv.2210.06453 (2022).
45. Heilbronner, S. R. & Hayden, B. Y. Dorsal Anterior Cingulate Cortex: A Bottom-Up View. *Annu. Rev. Neurosci.* **39**, 149–170 (2016).
46. Holroyd, C. B. & Verguts, T. The Best Laid Plans: Computational Principles of Anterior Cingulate Cortex. *Trends Cogn. Sci.* **25**, 316–329 (2021).
47. Kolling, N., Behrens, T. E. J., Mars, R. B. & Rushworth, M. F. S. Neural Mechanisms of Foraging. *Science* **336**, 95–98 (2012).

48. Wang, J. X. *et al.* Prefrontal cortex as a meta-reinforcement learning system. *Nat. Neurosci.* **21**, 860–868 (2018).
49. Blanchard, T. C. & Gershman, S. J. Pure correlates of exploration and exploitation in the human brain. *Cogn. Affect. Behav. Neurosci.* **18**, 117–126 (2018).
50. Behrens, T. E. J., Woolrich, M. W., Walton, M. E. & Rushworth, M. F. S. Learning the value of information in an uncertain world. *Nat. Neurosci.* **10**, 1214–1221 (2007).
51. Chien, J. M., Wallis, J. D. & Rich, E. L. Abstraction of Reward Context Facilitates Relative Reward Coding in Neural Populations of the Macaque Anterior Cingulate Cortex. *J. Neurosci.* **43**, 5944–5962 (2023).
52. Monosov, I. E., Haber, S. N., Leuthardt, E. C. & Jezzini, A. Anterior Cingulate Cortex and the Control of Dynamic Behavior in Primates. *Curr. Biol.* **30**, R1442–R1454 (2020).
53. Akam, T. *et al.* The Anterior Cingulate Cortex Predicts Future States to Mediate Model-Based Action Selection. *Neuron* **109**, 149-163.e7 (2021).
54. Soviany, P., Ionescu, R. T., Rota, P. & Sebe, N. Curriculum Learning: A Survey. *Int. J. Comput. Vis.* **130**, 1526–1565 (2022).

Figures

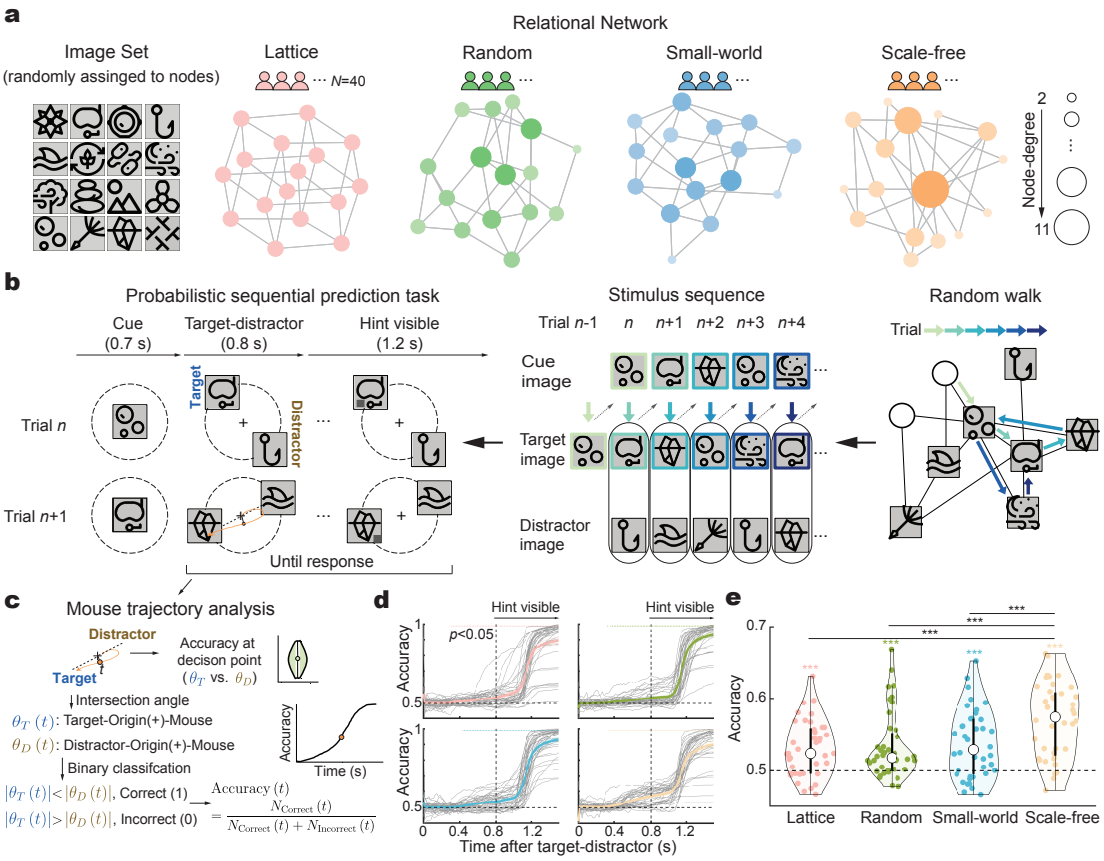

Figure 1. Network learning paradigm and behavioural performance (Experiment 1). a, Four groups learned four types of 16-node, undirected and unweighted transitional networks: Lattice (pink), Random (green), Small-world (blue), Scale-free (orange) networks with matched basic properties. Node-degree is denoted by node size and brightness. The same 16 black-and-white images (left) are randomly assigned to the 16 network nodes per subject. **b,** Sequential prediction task. Left: after cue image ("Cue"), subjects predict its succeeding image by mouse-clicking one of the two images ("Target-Distractor"). After 0.8 s, a gray square gradually appears on the target as a hint ("Hint visible"). Response before hint is encouraged and yields higher rewards. Middle: current-trial target image becomes the next-trial cue (dashed arrows). Right: target image sequence is generated via random-walk within corresponding network. Light green to dark blue arrows denote progression across trials. **c,** Time-resolved mouse trajectory analysis. Left: at each time point, angle between mouse cursor position and target and distractor images are computed as as $\theta_T(t)$ and $\theta_D(t)$, respectively. Smaller $\theta_T(t)$ than $\theta_D(t)$ indicates correct prediction and larger $\theta_T(t)$ than $\theta_D(t)$ indicates incorrect prediction. Accuracy (Accuracy(t)) is calculated as the proportion of correct classifications. Right: overall prediction accuracy at decision point. **d,** Time-resolved prediction accuracy of four networks. Gray and coloured lines denote individual subjects and grand average. Vertical dotted line indicates hint onset. Coloured dots on top indicate group-level significance (compared to 0.5 chance level; one-sample *t*-test, two-sided, $p<0.05$, *FDR* correction across time). **e,** Overall prediction accuracy of four networks. Coloured stars: above-chance accuracy within a group (compared to chance-level 0.5; one-sample *t*-test, two-sided). Black asterisks: post-hoc comparsion with Bonferroni correction between groups (GLMM1, ***: $p<0.001$).

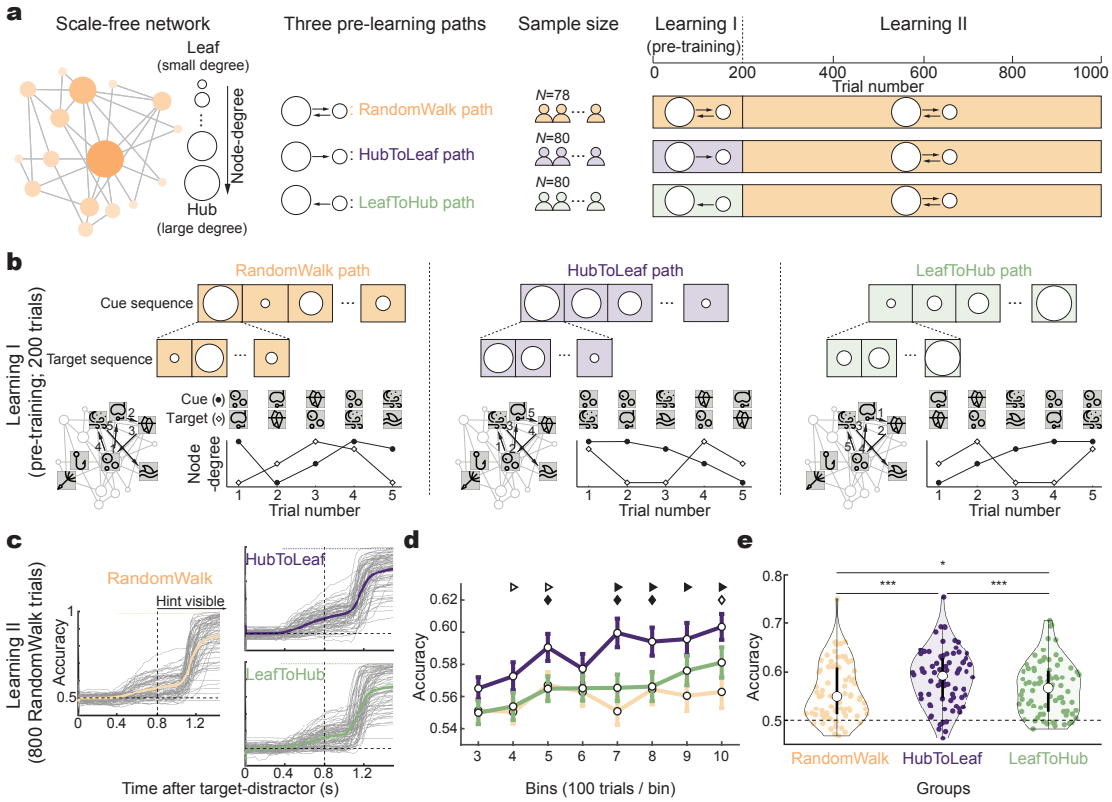

Figure 2. Compressive learning (Experiment 2). a, Left: inhomogeneity properties of scale-free network, containing Hub (large circle; more connections) and Leaf nodes (small circle; fewer connections). Middle: three pre-learning paths – RandomWalk (yellow), HubToLeaf (purple), LeafToHub (green). Right: during Learning I (200 trials), three groups learned sequences generated by different pre-learning paths (RandmWalk, HubToLeaf, LeafToHub). During Learning II (800 trials), they learned identical random-walk image sequences (yellow). Only learning II performance was compared between groups. **b,** Generation of three pre-learning paths (Learning I). Left: RandomWalk path is generated by 200-step random walks (arrows with number) visiting hub and leaf nodes in a mixed manner. Middle: HubToLeaf path is the reordering of the 200-length RandomWalk path based on cue and target images' node-degree in descending order. Right: LeafToHub path is the reordering of RandomWalk path in ascending order. The three pre-learning paths contain the same images with same frequencies but in different orders. **c,** Time-resolved prediction accuracy for three groups (Learning II). Gray and coloured lines denote individual subjects and grand average. Vertical dotted line indicates hint onset. Coloured dots on top indicate group-level significance (compared to 0.5; one-sample *t*-test, two-sided, $p<0.05$, *FDR* correction across time). **d,** Temporal evolution of prediction accuracy for three groups (Learning II). Triangle: HubToLeaf vs. Random; diamond: HubToLeaf vs. LeafToHub. Filled, $p<0.01$; hollow: $0.01\leq p<0.05$ (GLMM2 and Bonferroni corrected post-hoc comparisons in each time bin; *FDR* correction across bins). **e,** Overall prediction accuracy for three groups (Learning II). *: $0.01\leq p<0.05$; ***: $p<0.001$ (GLMM2 and post-hoc comparisons on all trials during Learning II).

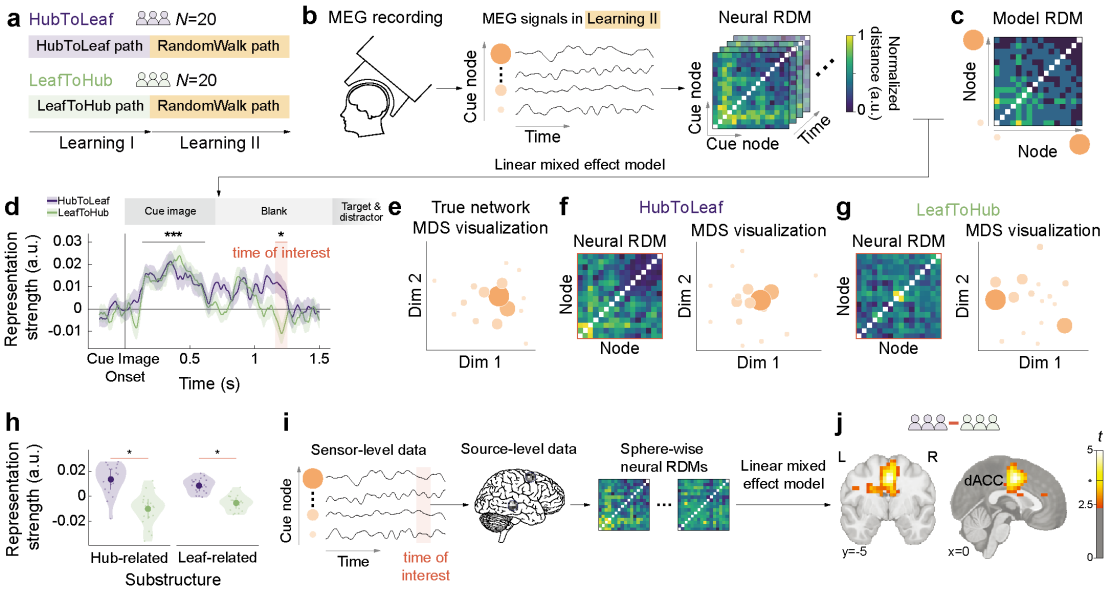

Figure 3. "Compressive learning" enhances network structure formation in dorsal ACC (Experiment 3, MEG). a, Two groups participated in Experiment 3 consisting of Learning I (200 trials; HubToLeaf or LeafToHub paths) and Learning II (600 trials; same RandomWalk path). Only Learning II is analysed. **b**, Each trial is labelled by the identity of cue image within network. Multivariate neural dissimilarities are calculated for all node pairs at each time point, resulting in time-resolved neural representational dissimilarity (neural RDM). **c**, Model RDM is constructed based on the corresponding minimal transitional distance within the network. Regressing Neural RDM by model RDM (linear mixed model, LMM1), yielding neural representational strength of network structure. **d**, Time-resolved neural representational strength of network structure during Learning II, for HubToLeaf (purple) and LeafToHub (green) groups (cluster-based permutation test; ***, $p < 0.001$; *, $p < 0.05$). Time window with significant group differences (shades in orange) is used as the time-of-interest for further analysis. **e**, Two-dimensional representation of the ground-truth network structure (multidimensional scaling of model RDM; MDS). Dots denote images within network. Dot size indexes node-degree. **f-g**, MDS of neural RDM within the time-of-interests for HubToLeaf and LeafToHub groups. **h**, Neural representational strength of sub-network structures – Hub-related and Leaf-related submatrix – within the time-of-interests, for HubToLeaf (purple) and LeafToHub (green) groups. **i**, Source-level analysis. Sensor-level data is projected into source space to perform the same RSA analysis within spheres of 5-mm radius. **j**, Searchlight results for HubToLeaf-LeafToHub group difference on neural representational strength of network structure (Whole-brain *t*-value map of group effect, LMM1; Asterisk in the colour bar: threshold of $p < 0.05$, *FDR* corrected).

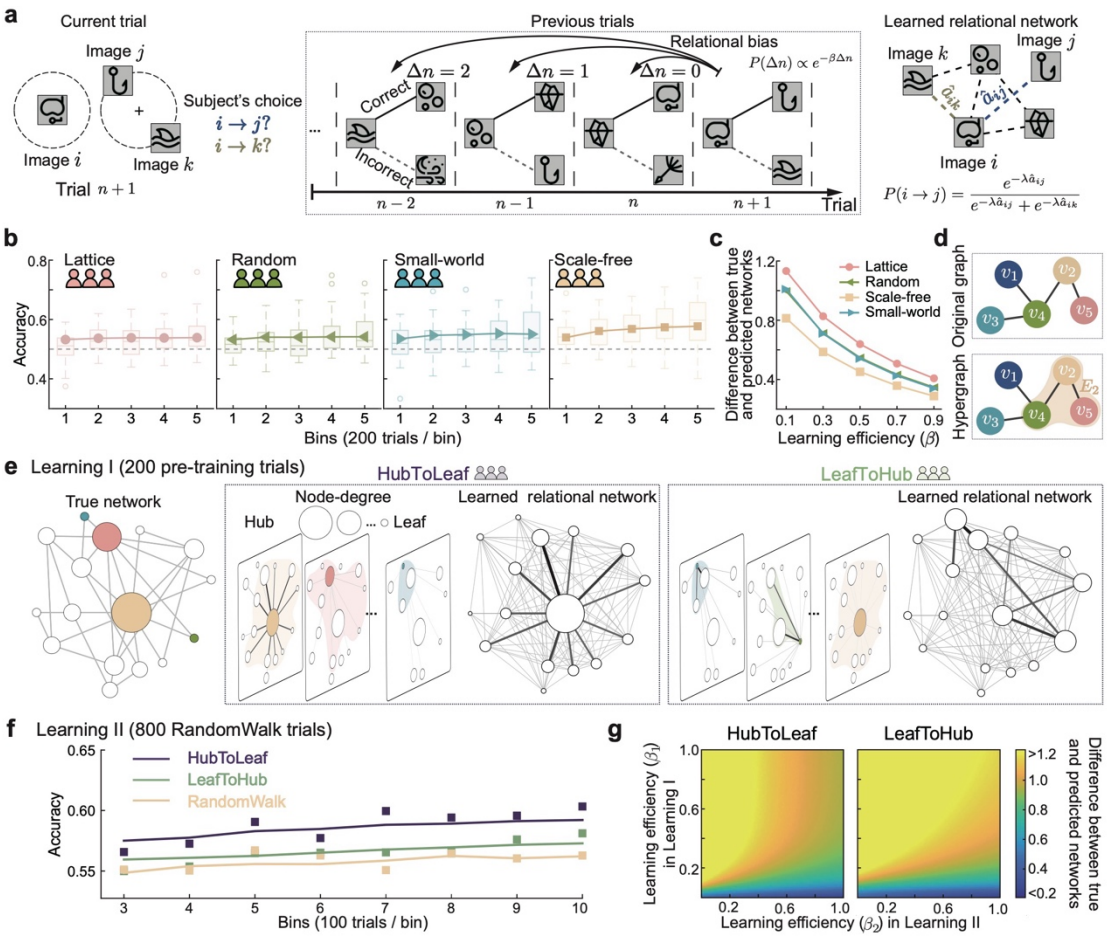

Figure 4. Theoretical model. a, Sequential prediction task (Experiment 1). Left: At trial $n+1$, subjects predict Cue image's (image i) succeeding image from Target-Distractor image pair, j and k, by retrieving and comparing their associations (*i.e.*, $i \to j; i \to k$) in memory. Middle: Associations between Cue (image i) and previously occurring images (e.g., images j, k) follow a Boltzmann distribution $P(\Delta n) = e^{-\beta \Delta n}$, with Δn denoting in-between trial interval. Right: Learned relational network, wherein associations between image i and image j, k (α_{ij} and α_{ik}) are compared to make a decision $P(i \to j)$. **b,** Model fitting (dark-coloured line) and behavioural data (light-coloured box plots) for four networks as a function of trial bins (200 trials per bin). **c,** Kullback-Leibler (KL) divergence between to-be-learned true network and learned network (5,000 simulations) as a function of β (lower value denotes better learning performance). **d**, Upper: Traditional graph theory. Lower: In the hypergraph, hyperedge E_i composes of node v_i and its all neighbors (shaded plane), e.g., E_2 contains v_2, v_4 and v_5. **e**, Illustration of hypergraph-based "compressive learning" during Learning I (Experiment 2). Left: To-be-learned network (**A**). Middle: For HubToLeaf pre-learning path, Hub-related hyperedge is first formed, followed by Leaf-related hyperedge, yielding the learned network ($\widehat{\mathbf{A}}_{\mathrm{h}}$). Right: For LeafToHub group, hyperedges are formed in a reversed order, from Leaf-related to Hub-related hyperedge. Note that $\widehat{\mathbf{A}}_{\mathrm{h}}$ formed via HubToLeaf path exhibits higher similarity to true network (**A**) than LeafToHub path. **f**, Model fitting (solid line) and behavioural performance (squared filled markers) during Learning II. **g**, Simulated learning performance (KL divergence) between true network and predicted learned network as a function of β_1 (learning I) and β_2(learning II), for HubToLeaf (left) and LeafToHub (right) paths (lower value denotes better performance). Values were truncated to [0.2, 1.2] for better visualisation.

Materials and Methods

Subjects.

The study had been approved by the Institutional Review Board of School of Psychological and Cognitive Sciences at Peking University (#2019-02-08). Subjects provided written informed consent in accordance with the Declaration of Helsinki.

Experiment 1

For the in-laboratory experiment, 20 human subjects (aged 18-30) of each group were recruited from Peking University. All of them had normal or corrected-to-normal vision. The behavioural experiment lasted for 60 min, and subjects received 55+(0~30) RMB for their time (basic participation fee + reward). For each group in the online experiment, 20 human subjects were recruited from the Prolific platform. The online experiment was decomposed into two sessions. Online subjects were allowed to participate in the 1st session if they were university students, aged between 18 and 30 years, fluent in English, and had an approval rate higher than 90. In the first session, subjects read the instructions and then completed a short examination to prove that they had fully understood the task. Only those subjects who passed the test within 5 attempts in the 1st session were invited to the 2nd session (the main experiment). The average completion time for the 1st and 2nd sessions was ~10 and ~50 min separately. In addition to the basic participation fee (£7.25), subjects had the opportunity to obtain an additional bonus (max. £4), which was accumulated across trials depending on their accuracy and RTs.

Experiment 2

78, 80 and 80 subjects from the Prolific platform were recruited for the RandomWalk, HubToLeaf, and LeafToHub groups in Experiment 2, respectively. Subjects who had participated in Experiment 1 were disqualified. For the in-laboratory experiment, 21 human subjects (aged 18-30) for each of the path group were recruited from Peking University.

Experiment 3

40 subjects (aged 18-30) were recruited from Peking University for the MEG experiment.

Apparatus and stimuli.

In-laboratory subjects were seated approximately 86 cm in front of a 21.5-inch iMac monitor (47.9×26.9 cm, 2,048×1,152 pixels, 60-Hz refresh rate). The display of stimuli and the recording of responses were controlled by the iMac computer using MATLAB R2017a and PsychToolbox-3[1,2]. The visual angle of each image was 2.25°, and all images in a display were equidistantly distributed on an invisible circle that subtended a visual angle of 9°. For the online experiment, the stimuli were presented in the unit ‘height’, defined as a relative measure to the height of the window. Thus, the physical sizes and

locations of the stimuli would change with different monitors. The stimuli were 16 cartoon images with abstract semantics (https://www.flaticon.com/packs).

Transition network

Unbeknownst to the subjects, we used four different transition networks (Figure 1a, top) in Experiment 1 to generate the image sequences across trials, with each node denoting one image in the image set (Figure 1a, left). The four networks were matched in their basic topological features, such as the same number of nodes (16) and edges (32), and an average node-degree (number of edges that are directly connected to the node) of 4. However, their node-degree distributions differed, resulting in diverse heterogeneity (Figure 1a, bottom). The Lattice network was a spherical shape, with each node fully connected to its adjacent four nodes. The Random network was generated based on the Erdős-Rényi model by randomly connecting each pair of nodes with the probability p, and the corresponding average degree of a random network was given by $p(N\text{-}1)$, where N is the total number of nodes[3]. The Small-world network was constructed by randomly rewiring the edges on regular (or Lattice) networks with the probability p=0.3[4]. In the current setting, the node-degree distribution of Random and Small-world network was similar to quasi-normal. The Scale-free network was constructed with the Barabási-Albert model[5], which possessed a unique feature of extremely high connectivity at very few nodes (the “hubs”). All subjects experienced the same 16 images and the same transition network within a group, but the correspondence between nodes and images was shuffled across subjects. Based on the objective transition network, four corresponding minimal distance matrices (MDM) were constructed, with each cell denoting the minimal transition steps between two nodes.

Probabilistic sequential prediction task

Each trial started with a cue image, followed by the presentation of target and distractor images (“Image onset”). The target image was directly connected to the cue image in the transition network (one-step transition), while the distractor images were more than one-step transitions from the cue image. In each trial, only one target image and one distractor image were displayed. Subjects’ task was to click the target image using the mouse as soon as possible after the image onset without sacrifice of accuracy, during which their time-resolved trajectories were recorded.

Experimental procedure

Each trial started with the cue image on the screen for 0.7 s (except for the 1st trial of each block, which was presented for 2 s), after which a one target and one distractor image were presented for 2 s (“Image onset”). The subjects’ task was to select the target image as accurately and quickly as possible through learning and feedback.

To facilitate the network learning, after 0.8 s presentations of alternative images, a small gray square (the ‘hint’) appeared gradually on the target image to indicate the correct

answer. Note that subjects were encouraged to make response before hint onset if they were confident. Once subjects made responses, auditory feedback was presented indicating whether the response was correct, incorrect, or time-out. The feedback screen lasted for 0.7 s.

Subjects received rewards on each trial based on their behavioural performances. Specifically, a correct response before hint would yield 100 virtual coins. Otherwise, the accessible coins decreased linearly with time, declining from 100 to 0 within 0.5 s and from 0 to -50 for the remaining 0.7 s. In other words, before- and after-hint responses yielded higher and lower rewards, respectively. Initially, subjects must rely on the hint, which appeared on the target image with the same gray scale as the background at 0.8 s and gradually increased to the largest gray scale within the next 0.8 s, to make a correct response. Otherwise, time-out or incorrect selection would lead to 50 coins loss. In the laboratory experiment, in order to control for the mouse moving speed, subjects were informed that the cursor's position would be forced back to the screen center if their moving speeds were too fast.

Generation of priming scenarios in Experiment 2 and 3

In Experiment 1, the target image in each trial served as the cue image in the next trial for subjects to make predictions, with the target image sequences being prescribed by a random walk on the transition network. A random walk is a path across a transition network created by taking repeated random steps between any two directly connected nodes[6]. In contrast, in Experiment 2 and 3, the continuity of the cue between target images across trials was broken for the first 200 trials. Specifically, the cue-target-distractor combination in each trial was ranked primarily based on the node-degree of cue image, and then ranked again based on the node-degree of target image under the same cue image (Figure 1c and 1d). Hence, the first 200 trials were sorted in descending order based on the node-degree of both the cue and target images for the HubToLeaf group. Conversely, in the LeafToHub group, the trials were sorted in ascending order. In summary, the three groups (Random, HubToLeaf, LeafToHub) differed only in their trial organisations in the first 200 trials ("priming scenarios"), while the stimulus exposure in the remaining 800 (Experiment 2) or 600 trials (Experiment 3) was similar. We therefore referred to the first 200 trials as the Learning I phase, and the remaining trials with random walk transitions as the Learning II phase. Subjects were not informed about the priming scenarios; they were only told that the cue image would be repeated over a period.

Time-resolved mouse trajectory analysis.

In the laboratory experiment, we recorded the mouse trajectory at a sampling rate of 60 Hz during each trial for each subject. The trajectory initiating from the center point and ending at the target image could reflect subjects' internal decision process. For the online experiment, we adjusted the sampling rate to 60 Hz by interpolation due to the different operating systems used by the subjects. At each sampling point within a trial, we calculated the absolute angle between the cursor dwell position (pixel unit for the in-laboratory

experiment and height unit for the online experiment) and each alternative image (target or distractor). A smaller absolute angle indicates a stronger decision preference towards a specific image.

To this end, we calculated the intersection angle between each sample point of the mouse trajectory and the center of the target or distractor images within a trial, with the center of the screen as the origin. The resulting mouse-origin-target angle (θ_t) and mouse-origin-distractor angle (θ_d) were then imported into a binary classifier to determine subjects' internal decision at the current sample point. Specifically, a correct choice was exported if the mouse's dwell position was closer to the target, i.e., $|\theta_t|<|\theta_d|$; otherwise, an incorrect response was output (Figure 1c, hollow arrows). By doing this, we transformed a continuous circular variable ($[-\pi, \pi]$) into discrete categorical variable (0 or 1). The accuracy at each sampling point was calculated as the proportion of trials classified into correct (choosing the target). To quantify the overall learning effect, we extracted one classification result from each trial. For the response-before-hint trials, the classification result at the point when subjects clicked the target was extracted. For the response-after-hint trials, the final landing position before the hint onset was used to make a classification (Figure 1c, filled arrows).

MEG Experiment.

Apparatus and MEG acquisition

Visual stimuli were presented with a projector (Panasonic PT-DS12KE) at a refresh rate of 60Hz. Auditory stimuli were presented with a pair of earphones. Subjects were seated in a magnetically shielded room and reacted with a MEG-compatible response box.

Neuromagnetic signals were recorded at 1,000 Hz by a 306-channel system (Elekta-Neuromag) with 102 magnetometers and 204 gradiometers while subjects were seated 1 m in front of a projection screen and performing the task.

MRI T1 data were acquired after MEG recording, using an MP-RAGE sequence on a Siemens 3T TRIO scanner, with voxel resolution of 1 × 1 × 1 mm^3 on a 176 × 192 × 192 grid (echo time = 2.98 ms, inversion time = 1,100 ms, repetition time = 2,530 ms).

Eye movement was monitored online by an eye tracker (Eyelink 1000 plus, remote mount) at 1000 Hz. Five-point calibration was performed every 100 trials.

MEG preprocessing

The preprocessing of MEG data was implemented with MNE-Python (version 1.3.1)[7], following the FLUX pipeline[8]. Maxwell filter and Signal-space separation were performed first to remove outside-helmet artifacts. The data were then high-pass filtered at 0.5 Hz and low-pass filtered at 40 Hz, followed by downsampling to 250 Hz. Independent component analysis was then performed on the filtered data. Ocular and cardiac components were manually identified for each subject and then subtracted from the data. All epochs were aligned at the onset of cue image. Only trials with correct responses were included for the following MEG analysis.

Representational similarity analysis (RSA)

The general principle of RSA is comparing the representational similarity between the neural activity and a proposed model[9].

The neural representation dissimilarity matrix (RDM) characterises the brain's responses. The neural RDM at time point t, $\mathbf{N}(t)$, is a 16×16 matrix. Each element of the neural RDM measures the dissimilarity of the neural representation between the node images. To obtain a robust estimate of the neural RDM, we performed a resampling procedure to balance the number of trials with different node images and repeated the resampling procedure 100 times. For each iteration, we randomly drew 50 trials with replacement from trials with the same cue image. The MEG data of the 50 trials were then averaged. We performed such drawing and averaging on the MEG data of each cue node. To obtain time-resolved neural RDMs, we calculated the Euclidean distance (1 - Pearson's *r*) between the topographic maps of different nodes at each time point. Then, we averaged RDMs from the 100 iterations. To de-noise the RDM, the RDM time series were subtracted with the average RDM over a baseline window (from the onset of cue image to 500 ms before the onset).

The MDM $\mathbf{M}$, a 16×16 matrix, characterises the underlying network structure[10]. Each element of the MDM denotes the step of the shortest path between two nodes according to the network graph.

To examine how the representation of network structure changes over time, we analysed the relationship between neural RDM and MDM at each time point. LMM1 were specified to test whether the subjects represent the network structure and whether group difference exists in representation strength. Cluster-based permutation test was used for correction (see SI for details).

For visualisation, neural RDMs and MDM are normalised and then projected to 2-dimensional Euclidean space with multidimensional scaling. Multidimensional scaling tries to reconstruct the coordinates of all nodes on a Euclidean map that minimize the summed absolute difference between the distance in dissimilarity matrices and the reconstructed distance. Multidimensional scaling is implemented with python package *sklearn*[11].

Leaf-related and hub-related submatrices

In the Scale-free network, nodes with more than 7 connections are defined as hub nodes, and the rest nodes are defined as leaf nodes. In Experiment 3, to examine whether path effect influences the entire network, we fitted LMM1 fitted separately on hub-related and leaf-related submatrices. Both submatrices are subset of a full dissimilarity matrix. Leaf-related submatrix contains only distances between leaf nodes. Hub-related submatrix is the complement set of leaf-related submatrix, which contains hub distances to both hub and leaf nodes.

Source-level RSA searchlight

Sensor-level signals within the two effective time windows (50-ms width, centered at 370 ms and 1196 ms) were projected to an average brain, respectively. Voxels were evenly

spaced 5 mm apart. The same RSA with minor modifications was then performed with researchlight at the radius of 10 mm (see SI for details).

Statistical Analysis

Linear mixed models (LMM) and generalised linear mixed models (GLMM) were implemented for group-level inference to account for both group-level and participant-level variance and to control nuisance variables. Both variables of interest and variables for control are specified as fixed effects. Specification of random effects followed the "keep-it-maximal" principle to prevent false positive results[12,13]. Random effects and their correlations would be reduced gradually in case of singularity. Recency of nodes, node-degree of target nodes, and minimal distance of distractor nodes are controlled as fixed and random effects. While LMM assumes Gaussian distribution for noise, GLMM assumes binomial response noise. The models are fitted with maximum likelihood estimation. The significance of each fixed effect is determined by Welch-Satterthwaite *t* test for LMM and likelihood ratio test for GLMM. The Bonferroni correction is used in post-hoc comparison. Cluster-based permutation test is used for test in the RSA time course[14].

Theoretical model

Here we utilise a graph to conceptualise the connections (edges) between images (nodes) and represent how the images relate to each other by the adjacency matrix $\mathbf{A} = [a_{ij}] \in \{0,1\}^{s\times s}$, where s is the number of nodes. If images i and j have a connection, $a_{ij} = a_{ji} = 1$; otherwise, $a_{ij} = a_{ji} = 0$. Define the degree matrix $\mathbf{D} = \mathrm{diag}(d_1, \cdots, d_s)$, where $d_i = \sum_{j=1}^{s} a_{ij} = \sum_{j=1}^{s} a_{ji}$.

In Experiment 1, image sequences are generated based on a random-walk path on the underlying network with the corresponding transition probability matrix obtained by $\mathbf{T} = \mathbf{D^{-1}A}$. Following the work of Lynn et al.[15], it suggests that the relational biases are inevitable for human subjects (Figure 4a, middle). Consider a sequence of stimuli $\{x_1, x_2, \cdots, x_N, x_{N+1}\}$, where $x_i \in \{1,2,\cdots,s\}$ refers to the image label. At the end of N trials, subjects' biased count of edge (i,j) can be estimated by

$$\tilde{n}_{ij}(N) = \sum_{n=1}^{N}\left(\sum_{\Delta n=0}^{n-1} P(\Delta n)[i = x_{n-\Delta n}]\right)[j = x_{n+1}],$$

where $P(\Delta n) = 1/Z\, e^{-\beta\Delta n}$ represents the distribution of the relational bias with Z serving as a normalisation constant such that $\sum_{\Delta n} P(\Delta n) = 1$, and $[\cdot]$ is an indicator function, which takes a value of 1 if the equation within the bracket holds and 0 otherwise. The free parameter β indicates the learning efficiency of the human subjects. As $N \to \infty$, the relative connection weight of edge (i,j) can be obtained by dividing both sides by N, yielding that

$$\lim_{N\to\infty} \frac{\tilde{n}_{ij}(N)}{N} = \sum_{\Delta n=0}^{\infty} P(\Delta n)\langle[i = x_{n-\Delta n}][j = x_{n+1}]\rangle,$$

where $\langle\cdot\rangle$ denotes the expectation. For the random walk on the graph,

$$P([x_{n-\Delta n}][x_{n+1}=j]) = \pi_i\left(\mathbf{T}^{\Delta n+1}\right)_{ij},$$

where $\pi_i = d_i/\sum_j d_j$ means the stationary distribution of node i appearing in the random walk. It then follows that $\hat{a}_{ij} = \sum_{\Delta n} P(\Delta n)\pi_i(\mathbf{T}^{\Delta n+1})_{ij}$, where $\hat{a}_{ij}$ indicates the learned internal representation for the edge (i,j). We express this in a matrix form, i.e., $\widehat{\mathbf{A}} = \sum_{\Delta n} P(\Delta n)\mathbf{\Pi}\mathbf{T}^{\Delta n+1}$, where $\mathbf{\Pi}$ is a diagonal matrix with its ith entry π_i.

To convert subjects' internal beliefs into choice probabilities, we adopt the binomial logistic regression to predict the likelihood of selecting image i followed by image j, not image k (Figure 4a, right)

$$P(i \to j) = \frac{1}{1+e^{-\lambda(\hat{a}_{ik}-\hat{a}_{ij})}},$$

where λ is a free parameter for the inverse temperature to capture choice randomness.

In Learning I of Experiment 2, the stimulus sequence establishes a cohesive learning unit that maps out the connection relation between a node and its neighbours. Human subjects, through these units, form the coarse-grained representation of the underlying network, beyond the dyadic network learning. We rely on the framework of hypergraphs, a potent tool in network science, to capture the process by modelling the basic units as hyperedges and constructing the weighted adjacency matrix to enable the extraction of higher-order network features (Figure 4d). Further, the coupling strength between nodes i and j in a hyperedge is not merely a binary value but depends on the involved dynamics[16]. We consider that the coupling strength between nodes in a hyperedge is relevant to the importance of nodes, which is intuitively described here in terms of the frequency of occurrence during the compressive learning process. Since normalisation is influenced by the relative, rather than the absolute value of the occurrence frequency, we denote the coupling strength between nodes i and j by $K_{ij} = \sum_\alpha k_{i\alpha}e_{i\alpha}\,k_{j\alpha}e_{j\alpha}$, where $e_{i\alpha} \in \{0,1\}$ indicates whether node i is in the hyperedge E_α, and $k_{i\alpha} = d_i$ if $i = \alpha$, otherwise 1. Therefore, we can derive the newly formulated incidence matrix with $\tilde{e}_{ii} = d_i$ and otherwise $\tilde{e}_{i\alpha} = e_{i\alpha}$. The adjacency matrix of the hypergraph can be represented by $\mathbf{A}_\mathrm{h} = \tilde{\mathbf{e}}\tilde{\mathbf{e}}^\mathrm{T}$ (Figure S14). Above is given the higher-order characterisation without considering the effect of local stimulus order on the learned network structure. Due to mental error and resource constraints, a node with a preceding stimulus order has fewer confounders and higher quality in learning its local structure, a phenomenon termed "primary effect" in cognitive science. We specify that the stimulus order of nodes $1,\cdots,s$ is represented by $o_1, o_2, \cdots, o_s$, and $\Omega_i = \{j: o_j < o_i\}$ denotes the set of nodes before node i in the order of stimuli. Further, we assume that

$$\widehat{\mathbf{A}}_h^l = e^{-\sum_{j\in\Omega_l}\beta d_j}\mathbf{A}_h^l,$$

where $\widehat{\mathbf{A}}_h^l$ and $\mathbf{A}_h^l$ indicate the learned local connection structure of node l when the local stimulus order is considered and not considered, respectively. Moreover, the diagonal elements are purposefully set to zero because the network topology does not contain self-edges.

Subsequently, in Learning II, the global features of the network structure can be observed by random-walk stimuli. Given the mixture effect of two learning phases, we

define the parameter $\alpha = n_l/(n_l + n_t)$ to account for the modulation in the learning process, where n_l denotes the number of trials of Learning I and n_t denotes the number of trials of Learning II. It allows us to derive an analytic expression for the learned network

$$\mathbf{C} = \alpha^p \widehat{\mathbf{A}}_{\mathrm{h}} + (1 - \alpha^p)\widehat{\mathbf{A}},$$

where the parameter p is used to measure the degree of nonlinearity in the modulation. Owing to factors such as task difficulty, learning efficiencies may not necessarily be the same in two learning phases. Thus, in order to differentiate, we use β_1 to indicate the learning efficiency for Learning I and β_2 for Learning II.

References

1. Brainard, D. H. The Psychophysics Toolbox. *Spat. Vis.* **10**, 433–436 (1997).
2. Pelli, D. G. The VideoToolbox software for visual psychophysics: Transforming numbers into movies. *Spat. Vis.* **10**, 437–442 (1997).
3. Erdös, P. & Rényi, A. On the evolution of random graphs. in *The Structure and Dynamics of Networks* 38–82 (Princeton University Press, Princeton, 2006). doi:doi:10.1515/9781400841356.38.
4. Watts, D. J. & Strogatz, S. H. Collective dynamics of 'small-world' networks. *Nature* **393**, 440–442 (1998).
5. Barabasi, A. L. & Albert, R. Emergence of scaling in random networks. *Science* **286**, 509–512 (1999).
6. Newman, M. *Networks: An Introduction*. (Oxford University Press, 2010). doi:10.1093/acprof:oso/9780199206650.001.0001.
7. Gramfort, A. *et al.* MEG and EEG data analysis with MNE-Python. *Front. Neurosci.* **7**, (2013).
8. Ferrante, O. *et al.* FLUX: A pipeline for MEG analysis. *NeuroImage* **253**, 119047 (2022).
9. Kriegeskorte, N., Mur, M. & Bandettini, P. Representational similarity analysis - connecting the branches of systems neuroscience. *Front. Syst. Neurosci.* **2**, (2008).
10. Ren, X., Zhang, H. & Luo, H. Dynamic emergence of relational structure network in human brains. *Prog. Neurobiol.* **219**, 102373 (2022).
11. Pedregosa, F. *et al.* Scikit-learn: Machine Learning in Python. *J. Mach. Learn. Res.* **12**, 2825–2830 (2011).
12. Barr, D. J., Levy, R., Scheepers, C. & Tily, H. J. Random effects structure for confirmatory hypothesis testing: Keep it maximal. *J. Mem. Lang.* **68**, 255–278 (2013).
13. Bates, D., Kliegl, R., Vasishth, S. & Baayen, H. Parsimonious Mixed Models. *arXiv:1506.04967 [stat]* (2018).
14. Maris, E. & Oostenveld, R. Nonparametric statistical testing of EEG- and MEG-data. *J. Neurosci. Methods* **164**, 177–190 (2007).
15. Lynn, C. W., Kahn, A. E., Nyema, N. & Bassett, D. S. Abstract representations of events arise from mental errors in learning and memory. *Nat. Commun.* **11**, 2313 (2020).
16. Carletti, T., Fanelli, D. & Lambiotte, R. Random walks and community detection in hypergraphs. *J. Phys. Complex.* **2**, 015011 (2021).